Impact of volcanic stratospheric aerosols on diurnal temperature range in Europe over the past 200 years: Observations versus model simulations

Renate Auchmann,[1] Florian Arfeuille,[1] Martin Wegmann,[1] Jörg Franke,[1] Mariano Barriendos,[2] Marc Prohom,[3] Arturo Sanchez-Lorenzo,[4,5] Jonas Bhend,[6] Martin Wild,[4] Doris Folini,[4] Petr Štěpánek,[7] and Stefan Brönnimann[1]

Received 28 February 2013; revised 9 August 2013; accepted 12 August 2013; published 30 August 2013.

[1] We analyze the impact of stratospheric volcanic aerosols on the diurnal temperature range (DTR) over Europe using long-term subdaily station records. We compare the results with a 28-member ensemble of European Centre/Hamburg version 5.4 (ECHAM5.4) general circulation model simulations. Eight stratospheric volcanic eruptions during the instrumental period are investigated. Seasonal all- and clear-sky DTR anomalies are compared with contemporary (approximately 20 year) reference periods. Clear sky is used to eliminate cloud effects and better estimate the signal from the direct radiative forcing of the volcanic aerosols. We do not find a consistent effect of stratospheric aerosols on all-sky DTR. For clear skies, we find average DTR anomalies of −0.08°C (−0.13°C) in the observations (in the model), with the largest effect in the second winter after the eruption. Although the clear-sky DTR anomalies from different stations, volcanic eruptions, and seasons show heterogeneous signals in terms of order of magnitude and sign, the significantly negative DTR anomalies (e.g., after the Tambora eruption) are qualitatively consistent with other studies. Referencing with clear-sky DTR anomalies to the radiative forcing from stratospheric volcanic eruptions, we find the resulting sensitivity to be of the same order of magnitude as previously published estimates for tropospheric aerosols during the so-called "global dimming" period (i.e., 1950s to 1980s). Analyzing cloud cover changes after volcanic eruptions reveals an increase in clear-sky days in both data sets. Quantifying the impact of stratospheric volcanic eruptions on clear-sky DTR over Europe provides valuable information for the study of the radiative effect of stratospheric aerosols and for geo-engineering purposes.

Citation: Auchmann, R., et al. (2013), Impact of volcanic stratospheric aerosols on diurnal temperature range (DTR) in Europe over the past 200 years: Observations versus model simulations, *J. Geophys. Res. Atmos.*, *118*, 9064–9077, doi:10.1002/jgrd.50759.

1. Introduction

[2] Explosive tropical volcanic eruptions can affect climate and weather on many time scales and over large areas and are one of the major causes of natural climate variability [*Robock*, 2000]. The impact of single eruptions on climate depends on the stratospheric aerosol loading, its injection height, and its spatial distribution, which depends on the location and timing of the eruption [*Simkin and Siebert*, 1994; *Robock*, 2000; *Kravitz and Robock*, 2011]. However, climate impacts of single eruptions are limited to 1–3 years [*Saxena et al*., 1997; *Robock*, 2000; *Stenchikov et al*., 2002]. The dominant and best understood mechanism through which volcanic eruptions influence climate is the direct radiative perturbation [*Stenchikov et al*., 1998; *Robock*, 2000]. Secondary sulfate (H_2SO_4 plus H_2O) aerosols, which are formed within weeks after the injection of SO_2 into the stratosphere [*Warnecke*, 1991; *Bluth et al*., 1997], enhance the reflectance of solar radiation and as a consequence lead to a loss of energy at the Earth's surface [*Rampino and Self*, 1984]. Stratospheric aerosol loading also leads to more absorption of longwave radiation in the lower stratosphere, which heats up the aerosol layer and enhances downwelling longwave radiation. This results in a net cooling at the surface and a net warming in the stratosphere [*Robock*, 2000]. Various additional effects on climate can be triggered by explosive volcanic eruptions [see *Robock*, 2000; *Cole-Dai*, 2010; *Timmreck*, 2012].

Additional supporting information may be found in the online version of this article.

[1]Institute of Geography and Oeschger Centre for Climate Change Research, University of Bern, Bern, Switzerland.
[2]Department of Modern History, University of Barcelona, Barcelona, Spain.
[3]Catalan Meteorological Service, Barcelona, Spain.
[4]Institute for Atmospheric and Climate Science, ETH Zürich, Zurich, Switzerland.
[5]Department of Physics, University of Girona, Girona, Spain.
[6]CSIRO Marine and Atmospheric Research, Aspendale, Victoria, Australia.
[7]Global Change Research Centre AS CR, v.v.i., Brno, Czech Republic.

Corresponding author: R. Auchmann, Institute of Geography, University of Bern, Hallerstrasse 12, Bern CH-3012, Switzerland. (renate.auchmann@giub.unibe.ch)

2169-897X/13/10.1002/jgrd.50759

Table 1. List of Volcanic Eruptions[a]

Volcano, Location	Month/Year of Eruption	30°N–90°N AOD From *Crowley* [2008]		42.75°N–52.25°N AOD From *Arfeuille et al.* [2013]		Global Aerosol Mass (Tg) From *Gao et al.* [2008]
		[radiative forcing in W/m^2: −20(AOD)] Wyr Syr+1 Wyr+1		[radiative forcing in W/m^2: −20(AOD)] Wyr Syr+1 Wyr+1		[radiative forcing in W/m^2: [(−20)(0.02)(global aerosol mass)^(0.658)]
Unknown, Tropics[c]	2[c]/1809	0.26 (−5.2)	0.17 (−3.4)	0.08 (−1.6)	0.08 (−1.6)	0.05 (−1.0)	53.8 (−5.5)
Tambora, Sumbawa, Indonesia	4/1815	0.33 (−6.6)	0.29 (−5.8)	0.20 (−4.0)	0.07 (−1.4)	0.08 (−1.6)	0.05 (−1)	109.7 (−8.8)
Krakatau, Sunda Strait, Indonesia	8/1883	0.10 (−2.0)	0.17 (−3.4)	0.11 (−2.2)	0.04 (−0.8)	0.08 (−1.6)	0.07 (−1.4)	21.9 (−3.1)
Santa Maria, Guatemala	4/1902	0.04 (−0.8)	0.10 (−2.0)	0.08 (−1.6)	0.11 (−2.2)	0.19 (−3.8)	0.13 (−2.6)	3.2 (−0.9)
Katmai, Alaska, USA	6/1912	0.22 (−4.4)	0.11 (−2.2)	0.05 (−1.0)	0.31 (−6.2)	0.13 (−2.6)	0.05 (−1.0)	11 (−1.9)
Agung, Bali, Indonesia	3/1963	0.01 (−0.2)	0.01 (−0.2)	0.03 (−0.6)	0.03 (−0.6)	0.05 (−1.0)	0.03 (−0.6)	20.9 (−3.0)
El Chichón, Chiapas, Mexico	3/1982	0.13 (−2.6)	0.10 (−2.0)	0.06 (−1.2)	0.07 (−1.4)	0.08 (−1.6)	0.05 (−1.0)	14[b] (−2.3)
Pinatubo, Luzon, Philippines	6/1991	0.12 (−2.4)	0.13 (−2.6)	0.08 (−1.6)	0.10 (−2.0)	0.14 (−2.8)	0.09 (−1.8)	30 (−3.8)

[a]The timing of the eruption is provided in column 2. Columns 3–5 give seasonally averaged 30°N–90°N aerosol optical depth (AOD) values provided by *Crowley* [2008]. Columns 6–8 give 42.75°N–52.25°N average AOD values provided by *Arfeuille et al.* [2013]. Global aerosol mass from *Gao et al.* [2008] (Tg) is given in column 9. In all columns, radiative forcing (W/m^2) is provided in parentheses. The column "Wyr" presents values for the boreal or Northern Hemisphere winter (October–March) starting in the same year after the volcanic eruption, "Syr + 1" presents values for the summer (April–September) 1 year after the volcanic eruption, and "Wyr + 1" denotes the second winter (October–March) after the volcanic eruption. Names of volcanoes are taken from *Robock* [2000] and *Simkin and Siebert* [1994].

[b]No estimates given by *Gao et al.* [2008], estimates derived from *Bluth et al.* [1992].

[c]*Cole-Dai et al.* [2009].

[3] The decrease of shortwave radiation on the ground only affects the energy balance during daytime [*Saxena et al*., 1997; *Wild et al*., 2009; *Bristow and Campbell*, 1984]. During the nighttime and daytime, a slight increase in surface net radiation is expected from the presumably very small increase in downwelling longwave radiation. Together, this is expected to lead to a reduction in the diurnal cycle [or diurnal temperature range, DTR = daily maximum (Tx) minus daily minimum temperatures (Tn)]. Extensive investigations on all-sky DTR have addressed tropospheric aerosol forcing in, e.g., "global dimming" and "global brightening" studies [*Wild et al*., 2009] or studies of (asymmetric) long-term trends in Tx and Tn in the context of global warming [*Karl et al*., 1986; *Karl et al*., 1993]. They all use DTR because of its high sensitivity to changes in radiative forcing [*Travis et al*., 2002]. Being highly correlated to surface solar radiation (SSR) [*Liu et al*., 2004; *Makowski et al*., 2009], DTR may also be used to analyze the effect of stratospheric volcanic aerosols on climate.

[4] The study of volcanically induced climate perturbations in observations is important for clarifying and quantifying the radiative effect of stratospheric volcanic aerosols. These are one of the main natural forcings with the potential of causing major climate impacts (e.g., approximately 40% of the decadal variance of the Little Ice Age could be explained by volcanic forcing) [*Crowley*, 2000; *Hegerl et al*., 2003]. The results can also have relevance for geo-engineering purposes to assess possible impacts and options.

[5] However, to date, no study has attempted to determine the radiative forcing from volcanic eruptions through studying DTR (in all-sky and clear-sky conditions), neither in observations nor models. For example, *Saxena et al*. [1997] only studied the effect of stratospheric aerosols on daily temperature and DTR trends in the 3 years following the Pinatubo and El Chichón eruptions. *Saxena et al*. [1997] used monthly mean temperature data from the southeastern U.S. and found a widespread decrease in DTR, which they partly attribute to the aerosol radiative forcing. They only used 3 year periods before the volcanic eruptions as reference.

[6] Here we use DTR anomalies (compared with approximately 20 year long reference periods around each eruption, depending on data availability and homogeneity) for three consecutive 6 month long seasons after volcanic eruptions to evaluate the stratospheric volcanic aerosol radiative impacts. DTR is calculated from five approximately 200 year long daily Tx/Tn station records in Europe. Besides the radiative effect, volcanic aerosols can also affect clouds and in this way impact local climate. To better quantify the radiative effect, we additionally consider clear-sky-only conditions based on subdaily long-term cloud cover records. We further analyze changes in cloud cover after volcanic eruptions. In a final step, we compare our results from the observations with a 28-member (two of the original 30 members are corrupted) ensemble of European Centre/Hamburg version 5.4 (ECHAM5.4) general circulation model simulations.

[7] The paper is organized as follows. In section 2, we give information on the data and methods. In section 3, we present the results from the observations and the model. A discussion is provided in section 4. Conclusions are drawn in section 5. In addition, we provide supporting information containing detailed information on the observational records, their homogeneity, and the subsequent determination of the reference periods.

Table 2. Details of the Stations Used in This Study

Station	Country	Latitude	Longitude	Source	References
Geneva (GE)	Switzerland	46°13′N	6°8′E	DigiHom (ETH & MeteoSwiss), IDAWEB (MeteoSwiss)	*Füllemann et al*. [2011]; *Auchmann et al*. [2012]
Basel (BA)	Switzerland	47°33′N	7°34′E	DigiHom (ETH & MeteoSwiss), IDAWEB (MeteoSwiss)	*Bider et al*. [1958]
Prague (PR)	Czech Republic	50°5′N	14°25′E	ECA&D	*Brázdil and Budiková* [1999]; *Klein Tank et al*. [2002]; *Brázdil et al*. [2012]
Barcelona (BC)	Spain	41°17′N	2°4′E	Early data: Mariano Barriendos; ECA&D	*Rodríguez et al*. [2001]; *Klein Tank et al*. [2002]; *Trigo et al*. [2009]; *Prohom et al*. [2012]
Hohenpeissenberg (HP)	Germany	47°48′N	11°1′E	DWD	*Winkler* [2009]

2. Data and Methods

2.1. Volcanic Eruptions

[8] Table 1 lists the volcanic eruptions considered in the study. We use eight explosive stratospheric eruptions [*Robock*, 2000] of the past 200 years for which Tx, Tn or subdaily temperature series, and subdaily cloud cover observations are digitally available. Note that due to a period of missing observations at all stations, the large eruption of Cosigüina (Nicaragua) in 1835 is excluded from this study.

[9] To estimate the sensitivity of clear-sky DTR on stratospheric aerosol forcing or, in other words, to quantify the change of clear-sky DTR per volcanic aerosol forcing unit (i.e., °C change in clear-sky DTR per W/m^2), we require a data set of estimated stratospheric volcanic aerosol forcing for the listed eruptions. As a basis, we use 30°N–90°N averages of aerosol optical depth (AOD) at 550 nm provided by *Crowley* [2008; see also *Crowley and Unterman*, 2012] who translated sulfate accumulations in 22 Antarctic ice cores into AOD. The calibration was based on the 1991 eruptions of Pinatubo and Hudson. Growth and decay of aerosol radii were derived from satellite observation data of the Pinatubo eruption and scaled by microphysical calculations for larger eruptions [*Crowley and Unterman*, 2012]. To obtain radiative forcing (W/m^2) values, we convert the AOD values into radiative forcing by applying a scaling factor of −20 ("thus a 0.120 twelve-month mean AOD for Pinatubo in the 30°N–90°N sector translates into a 2.4 W/m^2 forcing," T. Crowley, personal communication, 2012; Table 2, columns 3–5). *Lacis et al*. [1992] were the first to propose such regression relations for the globe. We use the radiative forcing values converted with the AOD values from *Crowley* [2008] to quantify the clear-sky DTR change per unit volcanic aerosol forcing in the observations and compare it with the clear-sky DTR change per W/m^2 in the model because the stratospheric aerosol forcing in the ECHAM5.4 model is also based on the AOD data set from *Crowley* [2008]. Note that applying a scaling factor to the global mean AOD can only give a coarse estimate of the radiative forcing and that using this factor to scale seasonal, nonglobal AOD values adds further uncertainties (see also discussion).

[10] Various data sets of estimates of stratospheric aerosol loading or AOD are available and the difference among the data sets and hence the uncertainty of the estimates is considerable. Therefore, we include two other volcanic aerosol data sets for comparison (however, only for observational data because the radiative forcing in the model is based on the AOD from *Crowley* [2008]). The first data set consists of seasonal average AOD for 42.75°N–52.25°N from *Arfeuille et al*. [2013]. This is based on results from a two-dimensional aerosol microphysical model initialized using total sulfate injections derived from *Gao et al*. [2008]. In the same way as for *Crowley* [2008], we scale the AOD values by −20 for the conversion to radiative forcing. The second data set consists of total aerosol mass injected by eruptions from *Gao et al*. [2008]. These values were derived from 54 ice core records in both the Arctic and Antarctica. We convert the total aerosol masses to global mean AOD using the power law relationship from *Arfeuille et al*. [2013]: AOD(peak) = (0.02) (global aerosol mass from *Gao et al*. [2008] [Tg])^(0.658). This formula was derived from the mean relationship between the calculated AOD peak (global mean) after volcanic eruptions and the corresponding total mass from *Gao et al*. [2008]. The AOD peak value averaged over all latitudes is indeed closely linked to the total mass injected by the eruptions. The AOD values are then converted to radiative forcing using the −20 factor as described earlier. Note that contrary to the two other data sets used, here the AOD corresponds to the maximum global mean values after the eruptions, providing an estimate of the global volcanic forcing rather than a local and seasonal aerosol effect.

2.2. Temperature Data and Cloud Cover Observations

[11] The lack of long-term highly resolved station data sets, especially long-term subdaily cloud cover observations, has previously impeded studying the clear-sky DTR changes during the last two centuries. The importance of long-term daily and subdaily data and its applications in climate studies has been pointed out and shown by many authors [e.g., *Klein Tank and Können*, 2003; *Moberg et al*., 2003; *Kuglitsch et al*., 2010; *Auchmann et al*., 2012]. In recent years, several data digitalization and data collection activities have been initiated, for instance, in Barcelona or Switzerland [*Füllemann et al*., 2011]. Consequently, five subdaily 200 year long series, providing both subdaily temperature series and subdaily cloud cover, are available. Table 2 summarizes the five European stations used in this study. For the listed stations, long-term daily Tx/Tn measurements, reconstructed Tx/Tn from the fixed hour measurements for the early period (maximum/minimum thermometers had not yet been in use for continuous daily climate monitoring when the 1809 and 1815 eruptions occurred), or state observations (i.e., subdaily measurement of the current temperature taken at a certain time, T_{state}) as well as subdaily cloud cover observations are digitally available for the whole period (1799–2010) or at least the periods around the eruptions.

[12] We did not homogenize the temperature series. However, we studied all available metadata and station histories to identify changes in instruments, measurement techniques, relocations, etc., in order to determine homogeneous

subperiods that could be used as reference (e.g., periods of approximately 20 years without any change in instruments). In this study, we only analyze anomalies. Hence, we assume that inhomogeneities outside the reference periods do not affect our results. Note, however, that inhomogeneities in daily series can affect not only the mean but also higher-order moments. For studying DTR anomalies after the Tambora 1815 and unknown 1809 eruptions in the Barcelona temperature series and after the Tambora eruption in the Geneva temperature series, we used subdaily observations (morning and noon/afternoon measurements assumed to approximate the daily Tx/Tn, respectively; for more details see supporting information) because no Tx/Tn series are available. This introduces some uncertainties into the calculation of DTR because (especially in winter) the diurnal cycle is less regular [*van den Besselaar et al*., 2012]. However, because the observation times within these three subperiods using subdaily data did not change and we are only using anomalies, we can assume that uncertainties caused by using subdaily observations are of minor relevance.

[13] In addition to using reported changes from metadata, we visually inspected cloud cover series for inhomogeneities. At long-term stations, cloud cover categories, observers, and observation times have changed over time and may lead to inhomogeneities [*Moberg et al*., 2003; *Sanchez-Lorenzo et al*., 2012]. Because we are analyzing anomalies during short homogeneous subperiods in this study (see section 2.4), we do not have to rely on long-term homogeneous cloud cover series. Detailed information on the station histories and reported changes of the temperature and cloud cover records is provided in the supporting information.

2.3. Temperature and Cloud Cover Data From Model Simulations

[14] Model data are extracted from 28 ECHAM5.4 atmospheric general circulation model (AGCM) runs (out of 30 runs, 2 are corrupted) covering the period from 1600 to 2005 [*Bhend et al*., 2012]. The original model data are calculated on 31 levels (L31) with a T63 resolution, a Gaussian grid of approximately 1.875° × 1.875° resolution. The model simulations were forced by the following boundary conditions.

[15] Stratospheric aerosol forcing is based on a reconstruction from ice core measurements [*Crowley*, 2008; *Crowley and Unterman*, 2012] (more details provided in previous section 2.1) for four latitudinal bands and at a monthly resolution.

[16] Land surface conditions were derived from potential vegetation classes [*Ramankutty and Foley*, 1999] in regions that are not anthropogenically influenced. Elsewhere, the vegetation was changed to crop or grassland according to the land use reconstruction of *Pongratz et al*. [2008]. Solar irradiance from a reconstruction by *Lean* [2000] was used. Greenhouse gas data were derived from *Yoshimori et al*. [2010]. An ozone climatology describing zonal averages of ozone volume mixing ratios at pressure levels was used [Fortuin and Kelder, 1998 via the German Climate Computing Center/Max-Planck-Institute for Meteorology (DKRZ/MPIMET)]. Tropospheric aerosol forcing was based on the reconstructed aerosol loads provided by *Koch et al*. [1999]. Before 1875, the anthropogenic sulfate was scaled with the world population. Sea surface temperatures (SSTs) and sea ice were prescribed from the Hadley Centre Sea Ice and SST version 1.1 (HadISST1.1) [*Rayner et al*., 2003]. Before 1870, the *Mann et al*. [2009] annual SSTs reconstruction was superimposed with a seasonal cycle and El Niño–Southern Oscillation-related variability and sea ice was set to climatological values from HadISST1.1. Before 1870, no variability was added to the climatological sea ice nor were the SSTs at the ice edge smoothed [*Bhend et al*., 2012].

[17] For our analysis, we locate the five grid points in the model closest to the five observation stations. Note that the closest grid point for Barcelona is a coastal grid point with an 84% land portion. We extract the temperature maxima and minima of four consecutive 6-hourly maximum and minimum temperatures from these grid points, respectively. Then, we extract cloud cover for the same grid points at 6 and 12 UTC which closely approximates the timing of the cloud cover observations at the stations.

2.4. Reference Periods and Seasons Analyzed

[18] Base periods are determined for each station and volcanic eruption (see Table S2 in the supporting information). The periods can slightly differ for the same eruption for different stations due to data availability and homogeneity reasons. Due to large inhomogeneities in the temperature series, two very different reference periods are used around the Agung eruption for the five stations (see Text S2 in the supporting information). This folds some uncertainties into the analysis, since the two periods (around 1960 to 1990 and around 1940 to 1965) differ with respect to global warming and tropospheric aerosols. From each base period, we exclude volcanically perturbed years, i.e., the year of a volcanic eruption as well as the two following years. We assume that after approximately 3 years, the remaining volcanic effect has decreased to a level that does not influence the results. The remaining years are termed the reference period. We estimate the DTR anomalies and the change in cloud cover (the change in frequency of clear-sky days) after each volcanic eruption. For each station and eruption, we compare different seasons after a volcanic eruption with the respective seasons of the corresponding reference period. We analyze the first winter half-year after an eruption (Wyr), the summer half-year 1 year after the eruption (Syr + 1), and the second winter half-year after the eruption (Wyr + 1). The 6 month long periods (instead of 3 month long seasons) provide a sufficient number of clear-sky days after the volcanic eruptions and during the reference period in order to compute reliable clear-sky DTR annual cycles (see section 2.5). Note that alternatively increasing the number of clear-sky days by broadening the definition of clear-sky days (e.g., to classify days with larger cloud cover fractions as clear-sky conditions) could introduce uncertainties into the analyses due to cloud effects.

2.5. Estimation of Clear-Sky and All-Sky DTR Anomalies

[19] To isolate clear-sky days in the observations, we use the cloud cover series from the single stations. Six different cloud cover categorizations are used for various stations and/or different time periods [e.g., 9 categories (octas), 10 categories (octas with a ninth category denoting fog), and the original verbal descriptions being categorized into 6 categories (see supporting information)]. First, we analyze the frequency distributions of the cloud cover categories for every station and determine the thresholds for clear-sky conditions. At most, two categories (from any categorization) are used to determine clear skies.

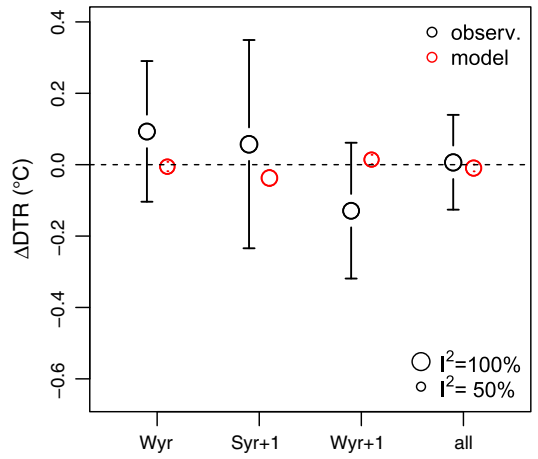

Figure 1. All-sky DTR changes for all stations (black) and associated grid points (red), with 95% CI, shown for the first winter (October–March, Wyr), the second summer (April–September, Syr + 1), the second winter (October–March, Wyr + 1) after a volcanic eruption, and for all of these seasons (all). The symbol size is scaled with I^2 (i.e., larger symbols indicate a larger amount of heterogeneity among the true effects).

[20] For the isolation of clear-sky days in the model grid points and the respective ensemble members, we use the average percentage of cloud cover of the 6 and 12 UTC cloud cover series. Based on a visual inspection of the distributions of the mean daily cloud coverage for various ensemble members and stations, we define cloud-free days as those with <10% average cloud cover (note that considering those with 0% would give too few cases).

[21] For the selected clear-sky days, we calculate the DTR as Tx minus Tn. From each reference period, we form a mean annual cycle for clear-sky DTR. To compute anomalies, we fit the first two harmonics (representing the seasonal cycle) to the reference periods and subtract the resulting mean values from the entire base periods (i.e., the reference years and the volcanically perturbed years after an eruption). We exclude single seasons and eruptions at stations (or grid points in the model) with less than four clear days in the season of interest (Wyr and Wyr + 1 in Basel for the Krakatau eruption in 1883, Wyr in Prague for the Santa Maria eruption in 1902, and Wyr + 1 in Prague for the Katmai eruption in 1912 are excluded from the observations and 462 seasons out of 2772 from the model).

[22] For determining DTR anomalies for all-sky conditions, we follow the same procedure detailed above for the observations and the model. However, instead of only clear-sky days, we use all days for the respective analysis.

[23] To estimate the mean clear-sky and the mean all-sky DTR effect (seasonally and over all events, with one "event" representing the mean DTR anomaly in one season at one station after one volcanic eruption or the mean DTR of one sample), we perform a meta-analysis [*Borenstein et al.*, 2007] using a random-effects model and compute a weighted mean (so-called combined effect) of the single-event means (instead of a simple mean), based on the total inverse variance (consisting of the sampling error and the variance between single seasonal station or ensemble member means). In contrast to assuming one "true effect" with a certain variance (e.g., fixed-effects model), the random-effects model accounts for additional variability between single events due to different sample characteristics [*Laird and Mosteller*, 1990; *Hedges and Vevea*, 1998; *Viechtbauer*, 2010]. Therefore, the combined effect is not assumed to represent the true effect (e.g., clear-sky DTR effect). Rather, the model assumes a true effect population, with the combined effect representing its mean μ. In other words, all of the observed effects T_i in a collection of k events or studies ($i = 1, 2, \ldots, k$; e.g., clear-sky DTR change for one event i) are sampled from a distribution with a certain true effect θ_i and a certain variance σ_i^2 (i.e., within-event variance, which heavily depends on the sample size of an event). However, those true effects are sampled from a distribution with mean μ and variance τ^2 (between-event variance) [*Hedges and Vevea*, 1998; *Borenstein et al.*, 2007, *Borenstein*, 2009]. The random-effects model thus reads [*Hedges and Vevea*, 1998; *Huedo-Medina et al.*, 2006; *Raudenbush*, 2009]

$$T_i = \theta_i + e_i, \tag{1}$$

$$\theta_i = \mu + u_i, \text{and} \tag{2}$$

$$T_i = \mu + u_i + e_i, \tag{3}$$

with $u_i \sim N(0, \tau^2)$ and thus the true effects being normally distributed (with mean μ and variance τ^2) [*Borenstein et al.*, 2007; *Borenstein*, 2009; *Viechtbauer*, 2010]. e_i is the within-study variability (quantified by the within-study variance σ_i^2). The average true-effect μ and the total heterogeneity among them τ^2 are being estimated. First, we estimate τ^2 using the restricted maximum-likelihood estimator [*Raudenbush*, 2009; *Viechtbauer*, 2010]. Then, we use weighted least squares to estimate μ, the weights w_i given by

$$w_i = 1/\left(\hat{\sigma}^2 + \hat{\tau}^2\right), \tag{4}$$

where $\hat{\sigma}^2$ is the within-event variance (sample variance) and $\hat{\tau}^2$ is the estimate of τ^2, the between-event variance. Confidence intervals (CIs) are obtained under the assumption of normality, with the standard error of the combined effect $\left(\overline{T}_i\right)$ being $\mathrm{SE}\left(\overline{T}_i\right) = 1/\sum_1^k w_i$ [*Borenstein et al.*, 2007].

[24] For testing the null hypothesis that there is homogeneity among the true effects, H_0: $\mu = 0$, and test H_0: $\tau^2 = 0$, we applied the Q test [*Hedges and Olkin*, 1985; *Viechtbauer*, 2010] to all meta-analysis in this study. The Q statistic [$Q = \sum_1^k w_i\left(T_i - \overline{T}_i\right)^2$, d.f. $= k - 1$] follows a normal distribution under H_0 [*Huedo-Medina et al.*, 2006]. For all combined effects in this study, the null hypothesis has to be rejected. In other words, all combinations of event means in this study (or pool of events, e.g., all Wyr events or events for one volcanic eruption) show large variability among the single-event means. Note that we base the decision to apply the random-effects model on the result of this homogeneity test (in contrast, homogeneity among the event means would have led to using the fixed-effects model).

[25] The I^2 index is used in this study to assess the total variability τ^2 [*Higgins and Thompson*, 2002; *Viechtbauer*, 2010]. I^2 measures the true heterogeneity and is interpreted as the percentage of variability due to the between-events variability and is directly related to τ^2 ($\hat{\tau}^2 = 0$, $I^2 = 0\%$)

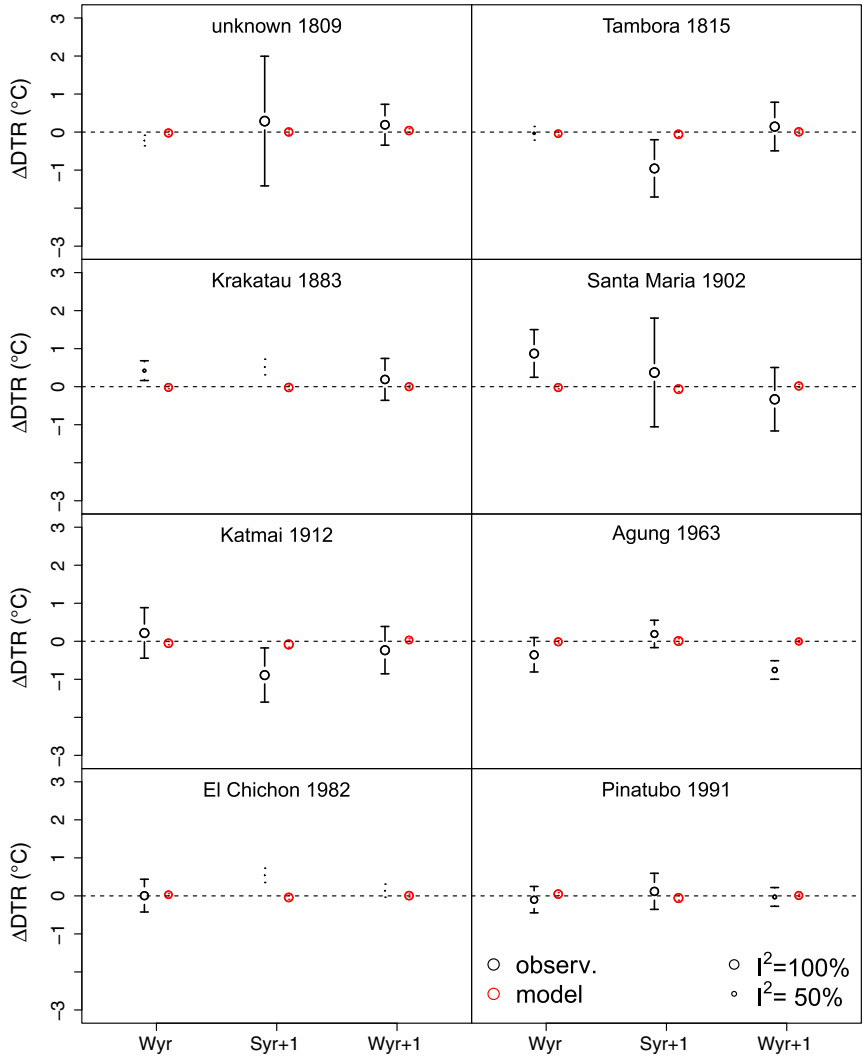

Figure 2. All-sky DTR changes by volcanic eruptions and seasons for all stations (black) and associated grid points (red), with 95% CI, shown for the first winter (October–March, Wyr), the second summer (April–September, Syr + 1), and the second winter (October–March, Wyr + 1) after a volcanic eruption. The symbol size is scaled with I^2 (i.e., larger symbols indicate a larger amount of heterogeneity among the true effects).

[*Huedo-Medina et al*., 2006]. The advantage of I^2 is that it is easy to interpret and does not depend on the degrees of freedom. This makes it ideal for meta-analysis using differing numbers of cases [*Higgins and Thompson*, 2002; *Huedo-Medina et al*., 2006], in contrast to τ^2, which can only be compared directly among samples of equal sizes.

[26] To quantify the sensitivity of clear-sky DTR on stratospheric volcanic aerosol forcing (the extent to which the magnitude of the volcanic aerosol forcing influences the clear-sky DTR effect, the average true effect), we fit a linear metaregression model [*Berkey et al*., 1995; *Viechtbauer*, 2012] and include radiative forcing (introduced in section 2.1 and Table 1) as moderator variable (or covariate) in the model (linear mixed-effects model) [*Borenstein et al*., 2007].

[27] The metaregression model has a fixed-effects term (e.g., representing a typical rate of change with respect to radiative forcing) and a random-effects term (e.g., describing variability due to different levels of the covariates, which are not assumed to be repeatable, but instead come from a random sample of levels in the population) [*Neter et al*., 1996] and is then given by

$$\theta_i = \beta_0 + \beta_1 x_{i1} + \cdots \beta_{p'} x_{ip'} + u_i, \tag{5}$$

where u_i is assumed to be normally distributed [$u_i \sim N(0, \tau^2)$]; τ^2 represents the amount of heterogeneity not explained by the moderators (residual heterogeneity); β_1, β_2,…, $\beta_{p'}$, are the fixed-effect coefficients (parameters); β_0 is a constant (intercept); p' is the number of moderators; and x_i are the covariates [*Viechtbauer*, 2010]. We first estimate τ^2 using the restricted maximum-likelihood estimator and then β_0, …, $\beta_{p'}$ using weighted least squares w_i [*Viechtbauer*, 2010]. Again, CIs for β_0,…, $\beta_{p'}$ are obtained under the assumption of normality.

[28] The R-package "metafor" is used to perform all meta-analyses [*Viechtbauer*, 2012].

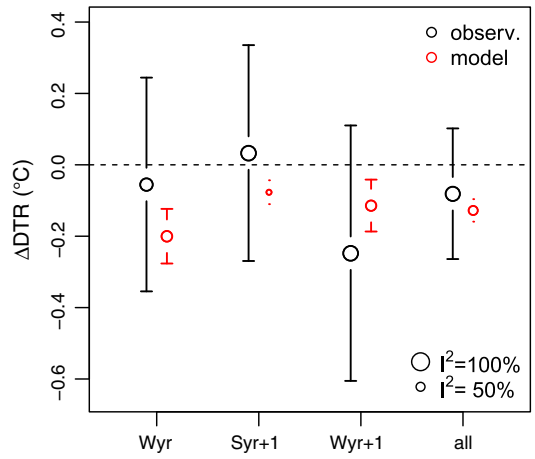

Figure 3. Clear-sky DTR changes for all stations (black) and grid points (red), with respective 95% CI, shown for the first winter (October–March, Wyr), the second summer (April–September, Syr + 1), the second winter (October–March, Wyr + 1) after a volcanic eruption, and for all seasons (all). The symbol size is scaled with I^2 (i.e., larger symbols indicate a larger amount of heterogeneity among the true effects).

2.6. Estimation of Cloud Cover Change

[29] In order to analyze the effect of volcanic eruptions on cloud cover, we calculate the clear-sky-day frequency anomalies between the reference seasons and the seasons after the volcanic eruptions.

[30] For studying significance at the event level, we use the chi-square test on a 2 × 2 contingency table. We determine the overall significance of the frequency anomalies for all events [treating all seasons, eruptions, stations, and (in the model case) ensemble members, independently] and for every season separately.

3. Results

3.1. All-Sky DTR Anomalies

[31] In a first step, we study the DTR anomalies for all days (including all cloudiness classes), all events combined, separate seasons, and single volcanic eruptions in the observations. We find almost no clear signal in all-sky DTR after volcanic eruptions for all events with a mean DTR anomaly of −0.007°C (±0.13°C, 95% CI; $p = 0.92$; see Figure 1, black symbols, "all"). For the single seasons after an eruption (Wyr, Syr + 1, and Wyr + 1), we find DTR anomalies of +0.09°C (±0.20°C, 95% CI; $p = 0.35$), +0.06°C (±0.30°C, 95% CI; $p = 0.70$), and −0.13°C (±0.20°C, 95% CI; $p = 0.18$), respectively (see Figure 1, black symbols), with the strongest signal found in Wyr + 1. The estimated amount of heterogeneity among the event means are large relative to the sampling error and yields $\tau^2 = 0.40$ for all events and $\tau^2 = 0.28$, $\tau^2 = 0.66$, and $\tau^2 = 0.26$, for the single-season Wyr, Syr + 1, and Wyr + 1, respectively. The corresponding (and directly comparable) I^2 values (Figure 1, circle sizes) are all around 90% or higher; for all events combined and for each season, meaning that almost all of the total variability can be attributed to the between-event variability, reflecting heterogeneous mean values for different stations and/or volcanoes and that only a small fraction of the total variability is caused by the sampling error.

[32] A combined analysis for single volcanic eruptions (see Figure 2, black symbols) reveals the largest negative anomalies for all-sky conditions (with $p < 0.05$) after the unknown eruption in 1809 (Wyr), after the Tambora eruption in 1815 (Syr + 1), after the Katmai eruption in 1912 (Syr + 1), and after the Agung eruption in 1963 (Wyr + 1).

[33] With respect to single events (i.e., one season at one station after one volcanic eruption, not shown) both significant increases and decreases of DTR are found (not shown) in the observations, reflecting the large heterogeneity among the events. The largest negative DTR anomalies are found in Geneva in Wyr after the 1815 Tambora eruption (1.79°C), in Hohenpeissenberg and Prague in Syr + 1 after the 1912 Katmai eruption (−1.73°C and −1.15°C, respectively), and in Hohenpeissenberg after the 1912 Katmai eruption in Wyr + 1 (−1.15°C) and the 1963 Agung eruption in Wyr + 1 (−1.03°C). The largest positive anomalies are found at Hohenpeissenberg in all three seasons after the Santa Maria eruption (1.78°C, 2.46°C, and 0.95°C, for Wyr, Syr + 1, and Wyr + 1, respectively) and after Krakatau (0.96°C in Wyr + 1). Another large positive anomaly is found in Prague in Syr + 1 (1.17°C) after the 1809 eruption.

[34] The results from the model for single seasons and all events combined (Figure 1, red symbols) and also for single volcanic eruptions (Figure 2, red symbols) show no signal. Note the very small confidence intervals because of the large number of data. However, there is also a notable spread among the single-model means (or true effects, see Figures 1 and 2, red symbols). All-days DTR anomalies are affected by many more changes with poorly understood underlying mechanisms including changes in cloud cover and its structure, tropospheric dynamics (e.g., mesoscale and small-scale dynamics) such as changes of weather type, and other possibly unknown (large-scale) mechanisms, which are triggered by volcanic stratospheric aerosols and likely influence the change of Tx and Tn (and thus DTR anomalies) after large eruptions. Also, additional longwave radiative and dynamical forcing may contribute to changes in DTR; however, the extent is unknown.

3.2. Clear-Sky DTR Anomalies

[35] Analyzing clear-sky DTR anomalies allows us to better estimate the signal from volcanic radiative forcing alone. Figure 3 shows the mean difference in clear-sky DTR anomalies for the three seasons and all events. In the observations (Figure 3, black symbols, "all"), we find an overall DTR decrease of −0.08°C (±0.18°C, 95% CI; $p = 0.39$) in clear-sky DTR, when comparing the mean clear-sky DTR after volcanic eruptions with the reference.

[36] For single events, different signs and magnitudes of significant clear-sky DTR anomalies are found (discussed below). This heterogeneity is also represented by the test statistics; the estimate of the amount of heterogeneity in the raw differences is $\tau^2 = 0.56$, with 80.1% of the total variability being attributed to the variability between the events ($I^2 = 80.1\%$). This is around 10% smaller than for the all-sky case, also pointing to a clearer signal on clear-sky days, although note that the percentage is still very high.

[37] Analyzing anomalies separately for each season (see Figure 3, black symbols) reveals negative anomalies for

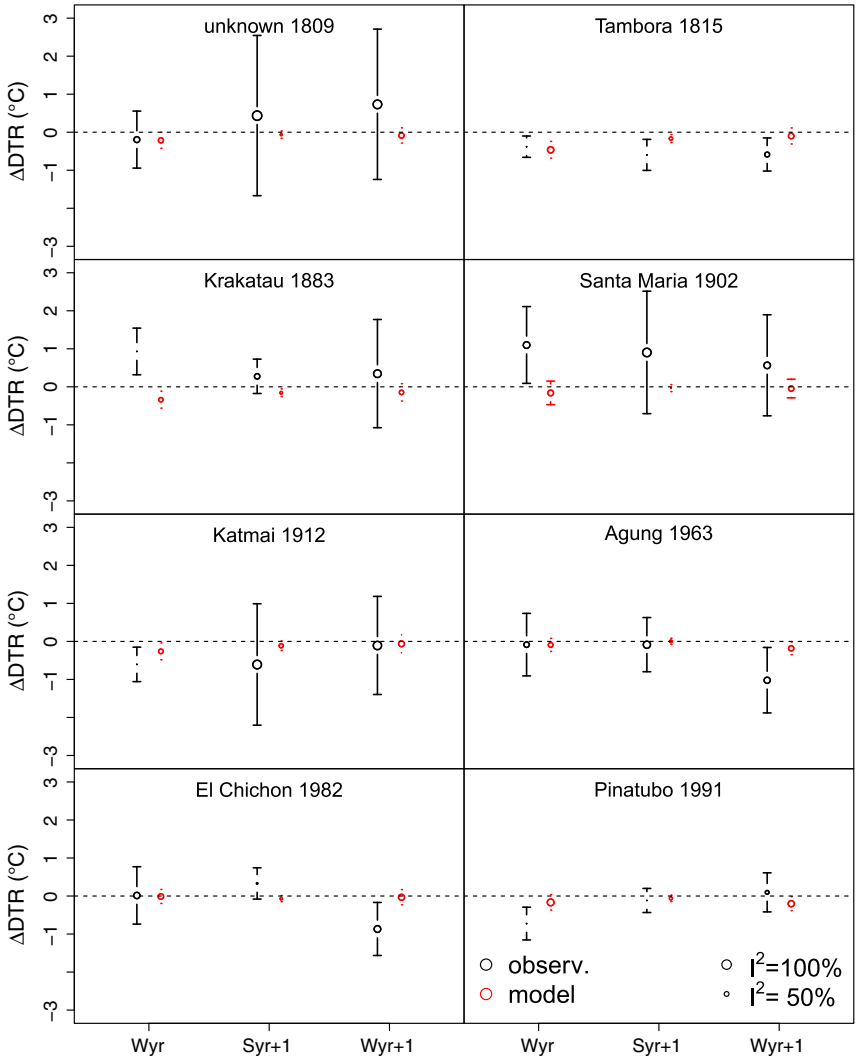

Figure 4. Clear-sky DTR changes by volcanic eruptions and seasons for all stations (black) and associated grid points (red), with 95% CI, shown for the first winter (October–March, Wyr), the second summer (April–September, Syr + 1), and the second winter (October–March, Wyr + 1) after a volcanic eruption. The symbol size is scaled with I^2 (i.e., larger symbols indicate a larger amount of heterogeneity among the true effects).

two seasons, with a larger signal found for the second winter after an eruption, Wyr + 1 (−0.25°C; ±0.36°C, 95% CI; $p = 0.18$). For Wyr, the mean DTR anomaly yields −0.06°C (±0.30°C, 95% CI; $p = 0.72$) and for Syr + 1 yields +0.03°C (±0.30°C, 95% CI; $p = 0.83$). The estimate of the amount of heterogeneity in the raw differences relative to the combined study over all events is only lower for Wyr with $\tau^2 = 0.42$ and $I^2 = 70.1\%$. Relative to the respective results of I^2 from the all-sky seasons, all clear-sky seasons yield a smaller fraction of variability due to the between-event variability. Note that an analysis of only the last 100 years (from Katmai 1912 onward) decreases the amount of heterogeneity and significance is reached for Wyr + 1 and for all seasons combined (not shown), which may reflect probable data quality issues of the very early data.

[38] Results from the model (Figure 3, red symbols) give negative results for all seasons and all events, with confidence intervals being 1 order of magnitude smaller than for the observations and all DTR changes being significant ($p < 0.05$). Also, more of the total variability in the model data can be attributed to the sampling error (instead of variability among the sample means) relative to the observations (Figure 3, compare circle sizes).

[39] With respect to single seasons at each station and for each volcanic eruption (not shown), we find the largest negative anomalies in the observations (all $p < 0.05$) in Geneva (−2.2°C in Wyr + 1 after the Agung 1963 eruption), in Basel (−2.1°C in Wyr + 1 also after the Agung eruption in 1963), and in Prague (−2.05°C in Syr + 1 and −1.97°C in Wyr after the Katmai 1912 eruption). In contrast to what is expected from reduced shortwave and increased longwave forcing, we also find significant positive anomalies. The largest positive (all $p < 0.05$) clear-sky DTR anomalies are found for Hohenpeissenberg (+1.99°C, +3.29°C, and +2.3°C in Wyr, Syr + 1, and Wyr + 1, respectively, all after the Santa Maria eruption in 1902) and in Geneva in Syr + 1 after the 1912 Katmai eruption (+2.0°C).

[40] Analyzing the combined effect of single volcanic eruptions for each season reveals the largest negative anomalies for clear-sky conditions in the observations (Figure 4,

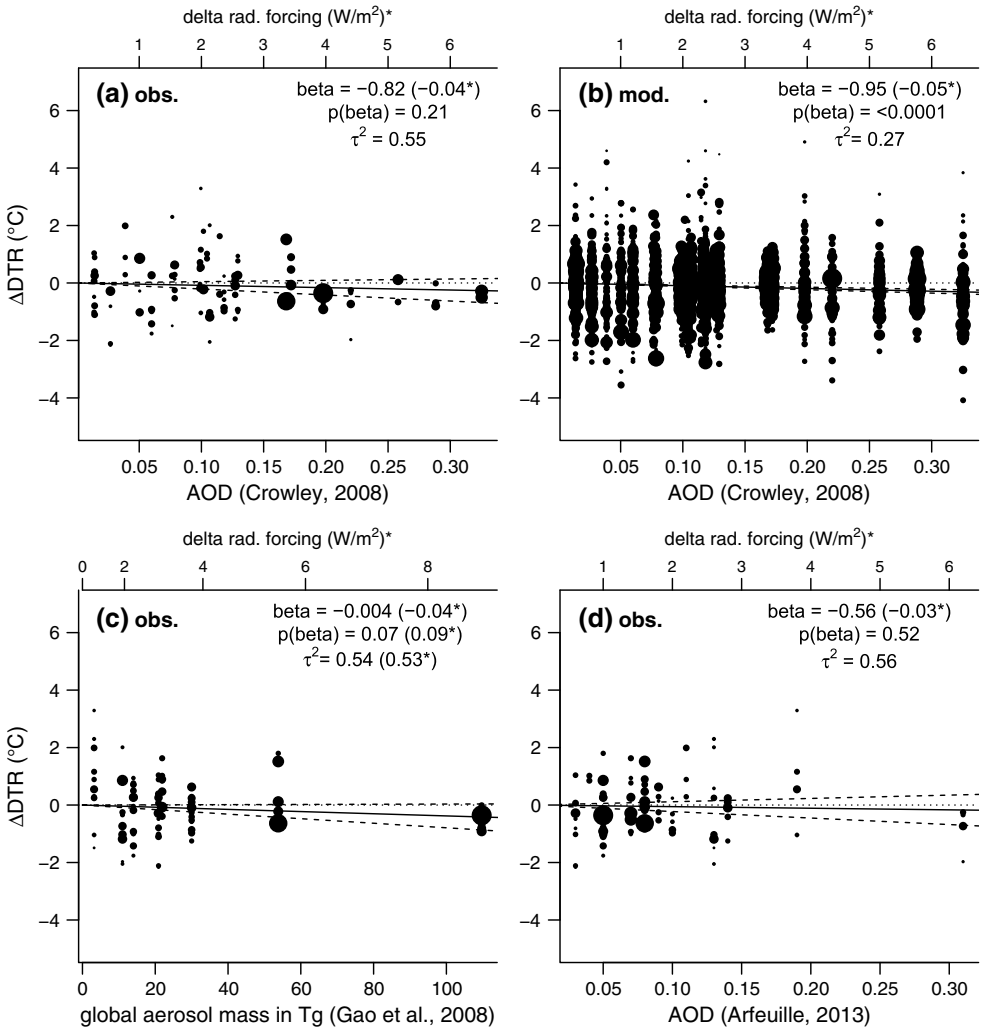

Figure 5. Clear-sky DTR changes as a function of AOD from *Crowley* [2008] in the latitudinal band 30° N–90°N and its conversion to radiative forcing using (a) observation and (b) model data. Clear-sky DTR changes from observation data as a function of (c) global aerosol amounts [*Gao et al*., 2008] and its conversion to radiative forcing and (d) 42.75°N–52.25°N averaged AOD [*Arfeuille et al*., 2013] and its conversion to radiative forcing. The intercept is set to zero for all models. Dashed lines represent the 95% CI bands and dotted lines mark the zero line. The symbol size is scaled with the respective weight w. The slope estimate (i.e., beta), its p-value [i.e., p(beta)], and the estimate of the residual heterogeneity τ^2 are indicated for the models using original values and for radiative forcing. Values indicate estimates with original values (AOD in Figures 5a, 5b, and 5d or global aerosol mass in Figure 5c; upper horizontal axis). Values in parentheses denoted by an asterisk indicate estimates using radiative forcing values. Note that for Figures 5a, 5b, and 5d, p-values and τ^2 estimates in parentheses are missing because the conversion from AOD to radiative forcing is a linear scaling. Thus, p-values for the slope estimate and τ^2 estimates are the same using AOD and radiative forcing.

black symbols) after the Tambora eruption in 1815 (all seasons with $p < 0.01$), after the Katmai eruption in 1912 (Wyr, $p < 0.01$), after the Agung eruption in 1963 (Wyr + 1, $p < 0.05$), after El Chichón (Wyr + 1, $p < 0.05$), and after Pinatubo (Wyr, $p < 0.01$).

[41] Model results for single volcanic eruptions (Figure 4, red symbols) generally show effects of reduced magnitude and with smaller confidence intervals. Except for the significant negative DTR change in the observations after El Chichón in Wyr + 1, all large negative changes from the observations mentioned above are also found in the model results. The largest discrepancies between model and observations are found for Krakatau (positive DTR changes in observations, negative ones in the model) and Santa Maria (positive DTR changes in observation, no clear signal in the model). However, we note large error bars in the observations.

[42] In a next step, we include AOD values (and AOD values converted to radiative forcing) as covariates in our regression model, which may account for some of the heterogeneity among the events in the clear-sky DTR anomalies. We use a linear mixed model and estimate regression coefficients by fitting four different models: (a) clear-sky DTR anomalies from observations with AOD values from *Crowley* [2008]

Table 3. Change in Absolute Frequency of Clear-Sky Days Compared With the Reference (Relative Change in Parentheses) in the Observation Data[a]

Volcano	Year	Station	Wyr	Syr + 1	Wyr + 1
Unknown	1809	BC	−4.4 (0.6)	−0.3 (1)	3.6 (1.3)
Unknown	1809	BS	—	—	—
Unknown	1809	GE	—	—	—
Unknown	1809	HP	—	—	—
Unknown	1809	PR	−4.9 (0.6)	8.1 (1.5)[b]	6.1 (1.4)
Tambora	1815	BC	7.6 (1.7)[b]	−8.3 (0.4)[b]	15.6 (2.4)[b]
Tambora	1815	BS	—	—	—
Tambora	1815	GE	−4.9 (0.8)	−13.7 (0.7)[b]	9.1 (1.4)
Tambora	1815	HP	—	—	—
Tambora	1815	PR	−8.9 (0.4)[b]	−5.9 (0.6)	−2.9 (0.8)
Krakatau	1883	BC	—	—	—
Krakatau	1883	BS	−14.6 (0.1)[b]	4 (1.1)	−14.6 (0.1)[b]
Krakatau	1883	GE	−2.9 (0.8)	−0.7 (1)	−1.9 (0.9)
Krakatau	1883	HP	10.1 (1.5)[b]	−0.3 (1)	11.1 (1.5)[b]
Krakatau	1883	PR	1.5 (1.1)	16.9 (1.7)[b]	12.5 (1.9)[b]
Santa Maria	1902	BC	—	—	—
Santa Maria	1902	BS	1.4 (1.1)	−9 (0.7)	−5.6 (0.6)
Santa Maria	1902	GE	10.7 (1.9)[b]	1.6 (1)	−5.3 (0.6)
Santa Maria	1902	HP	8.7 (1.4)	−7.4 (0.6)	−4.3 (0.8)
Santa Maria	1902	PR	1.8 (2.5)	4.9 (1.7)	2.8 (3.3)
Katmai	1912	BC	—	—	—
Katmai	1912	BS	8.9 (1.6)[b]	−5.4 (0.8)	2.9 (1.2)
Katmai	1912	GE	−6.4 (0.6)	−28.8 (0.2)[b]	−9.4 (0.3)[b]
Katmai	1912	HP	18.3 (1.8)[b]	13.1 (1.7)[b]	9.3 (1.4)[b]
Katmai	1912	PR	4.7 (4.6)[b]	−1.3 (0.8)	−0.3 (0.8)
Agung	1963	BC	0.6 (1)	2 (1.1)	17.6 (2.1)[b]
Agung	1963	BS	−5.9 (0.6)	10.7 (1.4)[b]	0.1 (1)
Agung	1963	GE	−6.9 (0.5)	−7.5 (0.8)	−7.9 (0.4)
Agung	1963	HP	2.9 (1.2)	4 (1.2)	−7.1 (0.6)
Agung	1963	PR	13 (1.8)[b]	16.4 (2.3)[b]	1 (1.1)
El Chichón	1982	BC	10.6 (1.7)[b]	6.8 (1.4)	8.6 (1.6)[b]
El Chichón	1982	BS	5 (1.3)	2 (1.1)	16 (2)[b]
El Chichón	1982	GE	8.2 (1.8)[b]	6.2 (1.2)	7.2 (1.7)[b]
El Chichón	1982	HP	6.3 (1.4)	0.9 (1.1)	4.3 (1.3)
El Chichón	1982	PR	−2 (0.9)	6.8 (1.7)[b]	9 (1.6)[b]
Pinatubo	1991	BC	8.1 (1.6)[b]	7.1 (1.6)	3.1 (1.2)
Pinatubo	1991	BS	10 (1.6)[b]	2 (1.1)	9 (1.6)[b]
Pinatubo	1991	GE	5.6 (1.5)	−1.8 (0.9)	7.6 (1.7)[b]
Pinatubo	1991	HP	7.3 (1.4)	4.9 (1.3)	5.3 (1.3)
Pinatubo	1991	PR	5.6 (1.5)	−1.8 (0.9)	7.6 (1.7)[b]
Seasonal averages			2.8 (1.2)[c]	1.7 (1.1)[c]	2.8 (1.2)[c]
Total average				2.8 (1.2)[c]	

[a]For expansion of station acronyms, consult Table 2.
[b]$p < 0.05$.
[c]$p < 0.01$.

(and radiative forcing converted with the AOD from *Crowley* [2008]), (b) clear-sky DTR anomalies from the model with AOD values from *Crowley* [2008] (and radiative forcing converted with the AOD from *Crowley* [2008]), (c) clear-sky DTR anomalies from observations with global aerosol mass [*Gao et al*., 2008] (and radiative forcing converted with global aerosol mass [*Gao et al*., 2008]), and (d) clear-sky DTR anomalies from observations with AOD from *Arfeuille et al*. [2013] (and radiative forcing converted with the AOD from *Arfeuille et al*. [2013]; for respective values see Table 1). We set the intercept to zero, assuming zero forcing during volcanically quiescent times.

[43] Figures 5a–5d show the metaregression lines for the clear-sky DTR anomalies and the covariates, together with the 95% CI bounds for the slopes. All panels show two horizontal axes: The lower horizontal axis shows the original covariates (AOD or aerosol mass) and the upper horizontal axis (denoted by an asterisk) shows the derived radiative forcing values (W/m^2). For a direct comparison, the slope estimates (beta, in parentheses denoted by an asterisk) for the metaregression models are calculated using the derived radiative forcing values (W/m^2). The slope estimates are also shown for the original units (AOD or aerosol mass, beta). Note that in Figure 5, for all AOD panels (Figures 5a, 5b, and 5d), the conversion from the original values to radiative forcing is only a linear scaling [−20(AOD)], so the *p*-values and τ^2 estimates are the same for the models using AOD or radiative forcing. For Figure 5c, the conversion from the global aerosol mass to radiative forcing is nonlinear (see section 2.1); hence, *p*-values and τ^2 estimates are given for the model using both global aerosol mass and using radiative forcing (in parentheses denoted by an asterisk) as covariate. The top panels show observation (Figure 5a) and model (Figure 5b) results for radiative changes derived with the AOD from *Crowley* [2008]. The slope estimates (beta*) yield $-0.041°C/W/m^2$ and $-0.048°C/W/m^2$ (Note that the units of the forcing, W/m^2, are shown as positive values throughout the paper for display purposes. However, forcing is negative per definition) for the observation and model data, respectively, with $p = 0.21$ for the observation-based slope estimate and $p < 0.001$ for the model-based slope estimate. Not only do the slope estimates have similar results, but the spread of both data sets is comparable despite having fewer observations (leading to higher τ^2 values). Interestingly, the data spread in the model is considerable for very large eruptions. A coarse estimate of the stratospheric volcanic aerosol effect on clear-sky DTR can hence be stated as −0.04 (reaching up to −0.05 in the model) $°C/W/m^2$ (negative forcing), which will be compared with other forcings from literature (see discussion provided in section 4).

[44] Additionally, we include two different aerosol data sets in our analysis, accounting for the uncertainty arising with estimating aerosol forcing data. Figures 5c and 5d show the metaregression lines for clear-sky DTR changes using radiative forcing converted with global aerosol mass from *Gao et al.* [2008] as moderator (Figure 5c) as well as using AOD from *Arfeuille et al*. [2013] shown in Figure 5d. All regression lines show similar slopes (from -0.03 to $-0.05°C/W/m^2$, see beta* estimates on the top right of Figures 5a–5d). In the observation-based models, a similar amount of variability (see τ^2 in Figures 5a, 5c, and 5d) is explained by the covariates with respect to the clear-sky DTR changes. For the observation-based metaregressions, there are not enough data points especially for large eruptions. Therefore, the regression lines are largely influenced by only few large eruptions, for instance, the high aerosol amounts (109.7 Tg; Figure 5c) in combination with the heavy weight of the Tambora eruption. Note that Tambora is much weaker in the *Arfeuille et al*. [2013] AOD data set (Figure 5d).

3.3. Changes in Clear-Sky Days

[45] To study the change in clouds after volcanic eruptions, we compare the mean frequency of cloud-free days after a volcanic eruption with the reference. The results from the analysis of observation data are presented in Table 3. We find a highly significant ($p < 0.001$) increase in clear-sky days after volcanic eruptions over all events (+2.8 days). Analyzing the seasons separately, we also find a significant increase for all seasons; Wyr, Syr + 1, and Wyr + 1 (+2.8, +1.7, and +3.8 days, respectively).

[46] However, the variability during different seasons and different volcanic eruptions is large (which is not surprising due to the large and unforced variability of cloud cover). We also find significant decreases in the frequency of clear-sky days. Interestingly, for Tambora in 1815, we find a negative change in all Syr + 1 for the three available stations, in accordance with the findings of *Auchmann et al*. [2012]. Furthermore, for the 1912 Katmai eruption, three out of five stations show negative changes in Syr + 1.

[47] Analyzing the frequency of clear-sky days from the model data also reveals positive changes. However, these changes are smaller than those from the observations. For Wyr, Syr + 1, and Wyr + 1, we find significant ($p < 0.01$) positive changes of +0.45, +0.5, and +0.85 days, respectively, resulting in an overall change of +0.6 days over all events.

4. Discussion

[48] We used subdaily meteorological data from five stations across central, western, and southwestern Europe as well as a 28-member ensemble simulation to analyze the impact of explosive stratospheric volcanic eruptions through radiative forcing on all-sky and clear-sky DTR for the first winter (Wyr), second summer (Syr + 1), and second winter half-year (Wyr + 1) after a volcanic eruption.

4.1. All-Sky DTR Anomalies

[49] Comparing all-sky DTR anomalies in the observation data after the eight largest volcanic eruptions during the instrumental period with our contemporary approximately 20 year reference periods reveals no clear combined DTR anomaly over Europe (−0.007°C; ±0.13°C, 95% CI). Seasonal analyses yield DTR anomalies of +0.09°C (±0.20°C, 95% CI), +0.06°C (±0.30°C, 95% CI), and −0.13°C (±0.20°C, 95% CI), for Wyr, Syr + 1, and Wyr + 1, respectively. Small DTR anomalies are also found when analyzing model data (e.g., overall effect yields −0.01°C), with much narrower confidence intervals due to the large amount of model data. The model- and observation-based results are not inconsistent, but also note that general circulation models (GCMs) tend to be insensitive with respect to changes in DTR. For example, *Wild* [2009] studied latest-generation GCMs [Intergovernmental Panel of Climate Change/Fourth Assessment Report – Coupled Model Intercomparison Project Phase 3 (IPCC/AR4-CMIP3)] and found a lack in decadal DTR variations. Also consult Stone and *Weaver* [2002, 2003] for an earlier GCM analysis.

[50] Besides tropospheric aerosols, clouds are one of the dominant factors for variations in SSR and DTR [*Wild*, 2009; *Ionita et al*., 2012]. To better estimate the volcanic aerosol radiative forcing alone, we eliminate the effect of clouds by repeating the analysis for clear-sky days, aware that additional effects, for instance, water vapor [*Wild et al*., 2007; *Wild*, 2009] or advection [*Karl et al*., 1993; *Wild et al*., 2007; *Makowski et al*., 2009] are not excluded.

4.2. Clear-Sky DTR Anomalies, Cloud Cover, and Mean Temperature Anomalies

[51] Analyzing observation data for clear-sky days results in a larger DTR change for all events of −0.08°C (±0.18°C, 95% CI; being 1 order of magnitude larger than the all-sky DTR change). For all seasons, DTR anomalies range from +0.03°C (Syr + 1; ±0.30°C, 95% CI) to −0.25°C (Wyr + 1; ±0.36°C, 95% CI). Note that the largest effect occurs in Wyr + 1 after the volcanic eruption. Comparing the clear-sky results from the observations with results from the model data gives similar (in terms of magnitude) results although the model gives slightly larger changes (e.g., overall clear-sky effect yields −0.13°C in the model). Again, confidence intervals are much narrower (around 1 order of magnitude smaller) around the model sample means due to the large amount of data and the fact that not all of the uncertainty can be captured by the model error bars. Hence, the error bars from the model and the observation cannot be directly compared. The similar results in the observations and the model suggest that if the forcings are appropriately represented in the model, the DTR response in the model seems to be adequate. It may indicate that the lack of DTR trends previously found in GCMs [see *Wild*, 2009, and references therein] is caused by a lack of (shortwave) forcing rather than an inappropriate land surface formulation (e.g., reproduction of soil moisture) [*Robock et al*., 2005; *Wild*, 2009].

[52] Comparing the heterogeneity among the events in the observations reveals a larger variance among the all-sky events, between the different seasons and different volcanic eruptions, than among the clear-sky events. This may be due to the better isolation of the stratospheric aerosol effect for clear-sky DTR, leading to a favorable signal-to-noise ratio. When analyzing all-sky DTR, cloud feedbacks distort and counteract the stratospheric aerosol primary radiative signal.

[53] Analysis of combined observations for single volcanic eruptions reveals the largest negative anomalies for all-sky and clear-sky conditions (with $p < 0.05$) after the Tambora eruption in 1815 (all-sky: Syr + 1; clear-sky: all seasons), after the Katmai eruption in 1912 (all-sky: Syr + 1; clear-sky: Wyr), and after the Agung eruption in 1963 (all-sky and clear-sky: Wyr + 1). Further negative changes (with $p < 0.05$) for clear-sky conditions only are found in Wyr + 1 after El Chichón and Wyr after Pinatubo and for all-sky in Wyr after the unknown eruption in 1809.

[54] The observation-based results for the largest volcanic eruption among those analyzed (i.e., in terms of estimated global aerosol loading), Tambora (in 1815), are consistent with many studies that show large impacts of the 1815 eruption (and also the 1809 eruption) on European weather and climate (e.g., "year without summer 1816") [*Self et al*., 1981; *Robock*, 1994, 2000; *Chenoweth*, 2009; *Trigo et al*., 2009; *Auchmann et al*., 2012]. Furthermore, the high-latitude volcanic eruption of Katmai in 1912 is well known for its climate effects in terms of, for instance, Northern Hemisphere summer cooling [*Oman et al*., 2005]. The significant decrease of clear-sky DTR in the first winter after Katmai also confirms the findings of *Kravitz and Robock* [2011]. Although in a simulation study of the Katmai eruption, *Kravitz and Robock* [2011] found that radiative forcing and AOD background levels were reached within 1 year after the eruption, still three out of four stations show a significant ($p < 0.05$) negative anomaly in Syr + 1 and one station (Hohenpeissenberg) also in Wyr + 1 after Katmai. However, for Syr + 1 the station Geneva and for Wyr + 1 the station Basel show significant positive anomalies, reflecting the large heterogeneity in the anomalies.

[55] Analyzing the change in absolute frequency of clear-sky days after stratospheric volcanic eruptions reveals a significant ($p < 0.001$) increase in clear-sky days over all events (+2.8 days) and all seasons in the observations and the model, with the largest increases in the two winter half-years, Wyr and Wyr + 1. For the whole domain, however, the results show a nonclear signal (both significant positive and negative changes) except for at the southernmost site, Barcelona, where the frequency of clear-sky days during post-volcanic winters following tropical eruptions was clearly enhanced. That finding is in clear agreement with the persistence of subtropical highs over southwestern Europe during these postvolcanic seasons [*Stenchikov et al*., 2002; *Fischer et al*., 2007; *Christiansen*, 2008] and could be the mechanism responsible for that increase. However, the large eruption of Tambora in 1815 yields a negative change in all Syr + 1 that in the case of Geneva, *Auchmann et al*. [2012] attribute to mesoscale circulation changes. Furthermore, decreases in the number of clear-sky days in Syr + 1 are found after the 1912 Katmai eruption (in three out of five available stations). An attribution study of causes for the overall increase in clear-sky days was not in the scope of this study.

[56] Analyzing DTR anomalies suggests the largest effect in Wyr + 1. In contrast, mean temperature anomalies [(Tx + Tn)/2] after stratospheric volcanic eruptions show a tendency toward a larger effect (cooling) in Syr + 1 after volcanic eruptions and a smaller cooling effect in the winters (all not reaching significance, not shown). This is in accordance with findings from literature (see, e.g., review study by *Robock* [2000], *Jones et al*. [2003], *Fischer et al*. [2007], and *Trigo et al*. [2009]) which provide confidence in the data used in this study. *Jones et al*. [2003] find for the Northern Hemisphere the largest cooling effect in Syr + 1 after tropical volcanic eruptions and little or no cooling effect for the winter month after volcanic eruptions. For the smaller region of central Europe, *Jones et al*. [2003] find no significant results. Also, *Fischer et al*. [2007] find over Europe a cooling effect in the first summer following 10 tropical eruptions; however, significance (<0.05) is reached only for the Fennoscandia region and not in central Europe. For the first winter following the 10 eruptions, *Fischer et al*. [2007] find a significant warming effect over northern Europe and only little or no effect (both cooling and warming) over central and southern Europe. Hence, extending the analysis of DTR anomalies to a larger region (e.g., Europe or the Northern Hemisphere, for a shorter period due to data availability) could potentially result in significance and then be compared to the response of mean temperatures after volcanic eruptions from literature.

[57] A regression analysis of clear-sky DTR anomalies and radiative forcing through stratospheric volcanic aerosols yields a change of -0.041°C/W/m^2 in clear-sky DTR from the observations and a similar result of -0.048°C/W/m^2 from the model data. However, note that the scaling of AOD to radiative forcing values shows important uncertainties, and hence here the derived change in clear-sky DTR per unit radiative forcing can only be a rough estimate. Additionally, applying this scaling to different latitudinal averages and different seasons adds further uncertainties. Accounting for the two seasons using a different scaling for the summer and winter seasons (because of the smaller radiative effect in Northern Hemisphere winters) may introduce some changes in the slope estimates of the regression lines. However, those changes are expected to be well below an order of magnitude. More reliable seasonal radiative forcing values for different latitudinal bands could potentially be obtained from radiative transfer modeling.

[58] *Makowski et al*. [2009] find seasonal (3 monthly) changes in DTR between -0.05 and -0.08°C/W/m^2 when analyzing 3 monthly DTR anomalies from 31 sites across Europe in the period 1970–2005 together with SSR data from the Global Energy Balance Archive database [*Gilgen and Ohmura*, 1999]. Note that *Makowski et al*. [2009] use all-sky DTR anomalies. Studies on changes in the SSR in the "global dimming" period [*Wild*, 2009] provide decadal trends over global land surface ranging from -2.3 to -5.1 W/m^2/decade during circa 1960–1990 (*Liepert* [2002] and *Stanhil and Cohen* [2001], respectively) and changes in DTR over global land surfaces from 1958 to 1985 on the order of -0.15°C/decade [*Wild et al*., 2007], resulting in a change of DTR ranging from -0.03 to -0.065°C/W/m^2 (note that we divided these values by $-$W/m^2 to acquire a negative sign for ease of comparison with our results). However, some (unknown) part of this change can be attributed to cloudiness. Comparing these values with the change in clear-sky DTR (from observations, this study) through stratospheric aerosol forcing of approximately -0.04°C/W/m^2 reveals that our findings are similar to the literature. We only considered clear-sky days. However, there could be an all-sky effect on the clear-sky DTR estimate in the sense that the temperature inertia after cloudy days may prevent an immediate full adjustment on consecutive clear-sky days to the clear-sky forcing. This memory effect in the temperatures on clear-sky days immediately following cloudy periods may underestimate the equilibrium clear-sky response and suggest that the -0.04°C/W/m^2 found in this study is an underestimate. Analyzing all-sky days, we find DTR sensitivity estimates of -0.001°C/W/m^2 in the observations ($p = 0.97$) and -0.005°C/W/m^2 in the model ($p < 0.01$). These estimates are 1 order of magnitude less than that found for clear-sky days and the above mentioned DTR sensitivities from tropospheric aerosol forcing in the global dimming period.

5. Conclusions

[59] We presented the first comprehensive study on the effect of radiative forcing through stratospheric volcanic eruptions on clear-sky and all-sky DTR over Europe based on long-term observations. A comparison of the observation based results with a 28-member model output yields comparable results in terms of magnitude and data spread with, due to the amount of model data, much narrower confidence intervals around the model-based estimates. Hence, additional long-term observation data are needed to consolidate statistical significance for the observation-based analysis. To quantify the climate response to stratospheric volcanic aerosol forcing, we use the clear-sky DTR as a physical measure. Although the resulting magnitudes of the clear-sky DTR changes after stratospheric volcanic eruptions are small, they correspond to the magnitudes of DTR responses to tropospheric aerosol forcing. Analyzing only clear-sky DTR allows for a better separation of the direct stratospheric aerosol effect from its feedbacks and

from other forcings. For geo-engineering measures involving sulfate aerosols, such results are relevant in order to test modeling results.

[60] **Acknowledgments.** This work is supported by the National Centre for Competence in Research (NCCR)-Climate program of the Swiss National Foundation (PALVAREX project) and under grant CRSI122-130642 (FUPSOL). MeteoSwiss is acknowledged for provision of data. We acknowledge the Catalan Meteorological Office (SMC, Barcelona, Spain) for providing funding support for the digitization of the Barcelona meteorological data series from 1780 to 2012. Computing facilities and time (for the paleosimulation with ECHAM5.4) were provided by the Swiss National Supercomputing Centre (CSCS). A.S.L. was supported by a post-doctoral fellowship from the government of Catalonia (2011 BP-B) and the project NUCLIERSOL (CGL2010-18546).

References

Arfeuille, F., D. Weisenstein, H. Mack, E. Rozanov, T. Peter, and S. Brönnimann (2013), Volcanic forcing for climate modeling: A new microphysics-based dataset covering years 1600–present, *Clim. Past Discuss.*, *9*, 967–1012.

Auchmann, R., S. Brönnimann, L. Breda, M. Bühler, R. Spadin, and A. Stickler (2012), Extreme climate, not extreme weather: The summer of 1816 in Geneva, Switzerland, *Clim. Past*, *8*(1), 325–335, doi:10.5194/cp-8-325-2012.

Berkey, C., D. Hoaglin, F. Mosteller, and G. Colditz (1995), A random-effects regression model for meta-analysis, *Stat. Med.*, *14*(4), 395–411.

van den Besselaar, E. J. M., A. M. G. Klein Tank, G. van der Schrier, and P. D. Jones (2012), Synoptic messages to extend climate data records, *J. Geophys. Res.*, *117*, D07101, doi:10.1029/2011JD016687.

Bhend, J., J. Franke, D. Folini, M. Wild, and S. Brönnimann (2012), An ensemble-based approach to climate reconstructions, *Clim. Past*, *8*(3), 963–976.

Bider, M., M. Schüepp, and H. Rudloff (1958), Die Reduktion der 200jährigen Basler Temperaturreihe, Archiv für Meteorologie, Geophysik und Bioklimatologie, Serie B, 9(3–4), 360–412, LA – German, doi:10.1007/BF02243047.

Bluth, G. J. S., S. D. Doiron, C. Schnetzler, A. Krueger, and L. Walter (1992), Global tracking of the SO_2 clouds from the June, 1991 Mount Pinatubo eruptions, *Geophys. Res. Lett.*, *19*(2), 151–154.

Bluth, G. J. S., W. I. Rose, I. E. Sprod, and A. J. Krueger (1997), Stratospheric loading of sulfur from explosive volcanic eruptions, *J. Geol.*, *105*(6), 671–684.

Borenstein, M. (2009), Effect sizes for continuous data, in *The Handbook of Research Synthesis and Meta-Analysis*, edited by H. Cooper, L. Hedges, and J. Valentine, 2nd Ed., pp. 221–235, Russell Sage Foundation, New York.

Borenstein, M., L. Hedges, J. P. T. Higgins, and H. Rothstein (2007), Introduction to meta-analysis, version 2, Biostat, Englewood, NJ, available at: http://www.meta-analysis.com (September 2012).

Brázdil, R., and M. Budiková (1999), An urban bias in air temperature fluctuations at the Klementinum, Prague, the Czech Republic, *Atmos. Environ.*, *33*(24–25), 4211–4217.

Brázdil, R., M. Bělínová, P. Dobrovolný, J. Mikšovský, P. Pišoft, L. Řezníčková, P. Štěpánek, H. Valášek, and P. Zahradníček (2012), Temperature and precipitation fluctuations in the Czech lands during the instrumental period, Masarykova univerzita, Brno, 236 s. ISBN 978-80-210-6052-4.

Bristow, K. L., and G. S. Campbell (1984), On the relationship between incoming solar radiation and daily maximum and minimum temperature, *Agr. Forest. Meteorol.*, *31*(2), 159–166.

Chenoweth, M. (2009), Daily synoptic weather map analysis of the New England cold wave and snowstorms of 5 to 11 June 1816, in *Historical Climate Variability and Impacts in North America*, edited by L.-A. Dupigny-Giroux and C. J. Mock, Springer, Netherlands, pp. 107–121.

Christiansen, B. (2008), Volcanic eruptions, large-scale modes in the Northern Hemisphere, and the El Niño–Southern Oscillation, *J. Climate*, *21*, 910–922, doi:10.1175/2007JCLI1657.1.

Cole-Dai, J. (2010), Volcanoes and climate, *WIREs Clim. Change*, *1*(6), 824–839, doi:10.1002/wcc.76.

Cole-Dai, J., D. Ferris, A. Lanciki, J. Savarino, M. Baroni, and M. H. Thiemens (2009), Cold decade (AD 1810–1819) caused by Tambora (1815) and another (1809) stratospheric volcanic eruption, *Geophys. Res. Lett.*, *36*, L22703, doi:10.1029/2009GL040882.

Crowley, T. J. (2000), Causes of climate change over the past 1000 years, *Science*, *289*(5477), 270–277, doi:10.1126/science.289.5477.270.

Crowley, T. J. (2008), Volcanism and the Little Ice Age, PAGES News 16, 22–23.

Crowley, T. J., and M. B. Unterman (2012), Technical details concerning development of a 1200-yr proxy index for global volcanism, *Earth Syst. Sci. Data Discuss.*, *5*(1), 1–28, doi:10.5194/essdd-5-1-2012.

Fischer, E. M., J. Luterbacher, E. Zorita, S. F. B. Tett, C. Casty, and H. Wanner (2007), European climate response to tropical volcanic eruptions over the last half millennium, *Geophys. Res. Lett.*, *34*, L05707, doi:10.1029/2006GL027992.

Fortuin, J., and H. Kelder (1998), An ozone climatology based on ozonesonde and satellite measurements, *J. Geophys. Res.*, *103*(D24), 709–734.

Füllemann, C., M. Begert, M. Croci-Maspoli, and S. Brönnimann (2011), Digitalisieren und Homogenisieren von historischen Klimadaten des Swiss NBCN – Resultate aus DigiHom, Arbeitsber. Meteo Swiss, Zürich, Switzerland.

Gao, C., A. Robock, and C. Ammann (2008), Volcanic forcing of climate over the past 1500 years: An improved ice core-based index for climate models, *J. Geophys. Res.*, *113*, D23111, doi:10.1029/2008JD010239.

Gilgen, H., and A. Ohmura (1999), The global energy balance archive, *Bull. Am. Meteorol. Soc.*, *80*(5), 831–850.

Hedges, L., and I. Olkin (1985), *Statistical Methods for Meta-Analysis*, Academic Press, San Diego, CA.

Hedges, L., and J. Vevea (1998), Fixed- and random-effects models in meta-analysis, *Psychol. Methods*, *3*(4), 486–504.

Hegerl, G. C., T. J. Crowley, S. K. Baum, K.-Y. Kim, and W. T. Hyde (2003), Detection of volcanic, solar and greenhouse gas signals in paleo-reconstructions of Northern hemispheric temperature, *Geophys. Res. Lett.*, *30*(5), 1242, doi:10.1029/2002GL016635.

Higgins, J., and S. Thompson (2002), Quantifying heterogeneity in a meta-analysis, *Stat. Med.*, *21*(11), 1539–1558, doi:10.1002/sim.1186.

Huedo-Medina, T., J. Sanchez-Meca, F. Marin-Martinez, and J. Botella (2006), Assessing heterogeneity in meta-analysis: Q statistic or I^2 index? Technical report, Center for Health, Intervention, and Prevention (CHIP) documents, University of Connecticut.

Ionita, M., G. Lohmann, N. Rimbu, and P. Scholz (2012), Dominant modes of diurnal temperature range variability over Europe and their relationships with large-scale atmospheric circulation and sea surface temperature anomaly patterns, *J. Geophys. Res.*, *117*, D15111, doi:10.1029/2011JD016669.

Jones, P. D., A. Moberg, T. J. Osborn, and K. R. Briffa (2003), Surface climate responses to explosive volcanic eruptions seen in long European temperature records and mid-to-high latitude tree-ring density around the Northern Hemisphere, in *Volcanism and the Earth's Atmosphere*, Geophys. Monogr. Ser., vol. *139*, edited by A. Robock and C. Oppenheimer, pp. 239–254, AGU, Washington, D. C., doi:10.1029/139GM15.

Karl, T., G. Kukla, and J. Gavin (1986), Relationship between decreased temperature range and precipitation trends in the United States and Canada, *J. Clim. Appl. Meteorol.*, *25*, 1878–1886.

Karl, T. R., P. D. Jones, R. W. Knight, G. Kukla, N. Plumme, V. Razuvayev, K. P. Gallo, J. Lindseay, R. J. Charlson, and T. C. Peterson (1993), Asymmetric trends of daily maximum and minimum temperature, *Bull. Am. Meteorol. Soc.*, *74*, 1007–1023.

Klein Tank, A. M. G., and G. P. Können (2003), Trends in indices of daily temperature and precipitation extremes in Europe, 1946–99, *J. Climate*, *16*(22), 3665–3680, doi:10.1002/joc.1163.

Klein Tank, A. M. G., et al. (2002), Daily dataset of 20th-century surface air temperature and precipitation series for the European climate assessment, *Int. J. Climatol.*, *22*(12), 1441–1453, doi:10.1002/joc.773.

Koch, D., D. Jacob, I. Tegen, D. Rind, and M. Chin (1999), Tropospheric sulfur simulation and sulfate direct radiative forcing in the Goddard Institute for Space Studies general circulation model, *J. Geophys. Res.*, *104*(D19), 23,799–23,822.

Kravitz, B., and A. Robock (2011), Climate effects of high-latitude volcanic eruptions: Role of the time of year, *J. Geophys. Res.*, *116*(D1), D01105, doi:10.1029/2010JD014448.

Kuglitsch, F. G., A. Toreti, E. Xoplaki, P. M. Della-Marta, C. S. Zerefos, M. Türkes, and J. Luterbacher (2010), Heat wave changes in the eastern Mediterranean since 1960, *Geophys. Res. Lett.*, *37*, L04802, doi:10.1029/2009GL041841.

Lacis, A., J. Hansen, and M. Sato (1992), Climate forcing by stratospheric aerosols, *Geophys. Res. Lett.*, *19*, 1607–1610, doi:10.1029/92GL01620.

Laird, N. L., and F. Mosteller (1990), Some statistical methods for combining experimental results, *Int. J. Technol. Assess. Health Care*, *6*(1), 5–30.

Lean, J. (2000), Evolution of the Sun's spectral irradiance since the Maunder minimum, *Geophys. Res. Lett.*, *27*(16), 2425–2428, doi:10.1029/2000GL000043.

Liepert, B. G. (2002), Observed reductions of surface solar radiation at sites in the United States and worldwide from 1961 to 1990, *Geophys. Res. Lett.*, *29*(10), 1421, doi:10.1029/2002GL014910.

Liu, B., M. Xu, M. Henderson, Y. Qi, and Y. Li (2004), Taking China's temperature: Daily range, warming trends, and regional variations, 1955–2000, *J. Climate*, *17*(22), 4453–4462, doi:10.1175/3230.1.

Makowski, K., E. Jäger, M. Chiacchio, M. Wild, E. Tracy, and A. Ohmura (2009), On the relationship between diurnal temperature range and surface solar radiation in Europe, *J. Geophys. Res.*, *114*, D00D07, doi:10.1029/2008JD011104.

Mann, M. E., J. D. Woodruff, J. P. Donnelly, and Z. Zhang (2009), Atlantic hurricanes and climate over the past 1,500 years, *Nature*, *460*, 880–883, doi:10.1038/nature08219.

Moberg, A., H. Alexandersson, H. Bergström, and P. D. Jones (2003), Were southern Swedish summer temperatures before 1860 as warm as measured?, *Int. J. Climatol.*, *23*, 1495–1521, doi:10.1002/joc.945.

Neter, J., M. H. Kutner, C. J. Nachtsheim, and W. Wasseman (1996), *Applied Linear Statistical Models*, McGraw-Hill, 4th ed., pp. 1408, Chicago, IL.

Oman, L., A. Robock, G. Stenchikov, G. A. Schmidt, and R. Ruedy (2005), Climatic response to high-latitude volcanic eruptions, *J. Geophys. Res.*, *110*(D13), D13103, doi:10.1029/2004JD005487.

Pongratz, J., C. Reick, T. Raddatz, and M. Claussen (2008), A reconstruction of global agricultural areas and land cover for the last millennium, *Global Biogeochem. Cycles*, *22*, GB3018, doi:10.1029/2007GB003153.

Prohom, M., M. Barriendos, E. Aguilar, and R. Ripoll (2012), Recuperación y análisis de la serie de temperatura diaria de Barcelona, 1780–2011, in *Cambio climático. Extremos e impactos, Publicaciones de la Asociación Española de Climatología*, Serie A, n° 8, edited by C. Rodríguez Puebla et al., pp. 207–217, AEC, Salamanca.

Ramankutty, N., and J. A. Foley (1999), Estimating historical changes in global land cover: Croplands from 1700 to 1992, *Global Biogeochem. Cycles*, *13*(4), 997–1027, doi:10.1029/1999GB900046.

Rampino, M. R., and S. Self (1984), Sulphur-rich volcanic eruptions and stratospheric aerosols, *Nature*, *310*, 677–679.

Raudenbush, S. (2009), Analyzing effect sizes: Random effects models, in *The Handbook of Research Synthesis and Meta-Analysis*, 2nd Ed., edited by H. Cooper, L. Hedges, and J. Valentine, pp. 295–315, Russell Sage Foundation, New York.

Rayner, N. A., D. E. Parker, E. B. Horton, C. K. Folland, L. V. Alexander, D. P. Rowell, E. C. Kent, and A. Kaplan (2003), Global analyses of sea surface temperature, sea ice, and night marine air temperature since the late nineteenth century, *J. Geophys. Res.*, *108*(D14), 4407, doi:10.1029/2002JD002670.

Robock, A. (1994), Review of the year without summer? World climate in 1816, *Clim. Change*, *26*, 105–108.

Robock, A. (2000), Volcanic eruptions and climate, *Rev. Geophys.*, *38*(2), 191–219, doi:10.1029/1998RG000054.

Robock, A., M. Mu, K. Vinnikov, I. V. Trofimova, and T. I. Adamenko (2005), Forty-five years of observed soil moisture in the Ukraine: No summer desiccation (yet), *Geophys. Res. Lett.*, *32*, L03401, doi:10.1029/2004GL021914.

Rodríguez, R., M. Barriendos, P. D. Jones, J. Martín-Vide, and J. C. Peña (2001), Long pressure series for Barcelona (Spain). Daily reconstruction and monthly homogenization, *Int. J. Climatol.*, *21*(13), 1693–1704, doi:10.1002/joc.696.

Sanchez-Lorenzo, A., J. Calbo, and M. Wild (2012), Increasing cloud cover in the 20th century: Review and new findings in Spain, *Clim. Past*, *8*, 1199–1212, doi:10.5194/cp-8-1199-2012.

Saxena, V. K., S. Yu, and J. Anderson (1997), Impact of stratospheric volcanic aerosols on climate: Evidence for aerosol shortwave and longwave forcing in the Southeastern U.S, *Atmos. Environ.*, *31*(24), 4211–4221.

Self, S., M. R. Rampino, and J. J. Barbera (1981), The possible effects of large 19th and 20th century volcanic eruptions on zonal and hemispheric surface temperatures, *J. Volcanol. Geotherm. Res.*, *11*(1), 41–60.

Simkin, T., and L. Siebert (1994), *Volcanoes of the World*, Geosc. Press, Tucson, Ariz.

Stanhil, G., and S. Cohen (2001), Global dimming: A review of the evidence for a widespread and significant reduction in global radiation, *Agr. Forest Meteorol.*, *107*, 255–278, doi:10.1016/S0168-1923(00)00241-0.

Stenchikov, G. L., I. Kirchner, A. Robock, H.-F. Graf, J. C. Antuña, R. G. Grainger, A. Lambert, and L. Thomason (1998), Radiative forcing from the 1991 Mount Pinatubo volcanic eruption, *J. Geophys. Res.*, *103*(D12), 13,837–13,857, doi:10.1029/98JD00693.

Stenchikov, G., A. Robock, V. Ramaswamy, M. D. Schwarzkopf, K. Hamilton, and S. Ramachandran (2002), Arctic oscillation response to the 1991 Mount Pinatubo eruption: Effects of volcanic aerosols and ozone depletion, *J. Geophys. Res.*, *107*(D24), 4803, doi:10.1029/2002JD002090.

Stone, D. A., and A. J. Weaver (2002), Daily maximum and minimum temperature trends in a climate model, *Geophys. Res. Lett.*, *29*(9), 1356, doi:10.1029/2001GL014556.

Stone, D. A., and A. J. Weaver (2003), Factors contributing to diurnal temperature range trends in twentieth and twenty-first century simulations of the CCCma coupled model, *Clim. Dynam.*, *20*, 435–445.

Timmreck, C. (2012), Modeling the climatic effects of large explosive volcanic eruptions, *WIREs Clim. Change*, *3*, 545–564, doi:10.1002/wcc.192.

Travis, D., S. Changnon, and R. Lauritsen (2002), Contrails reduce daily temperature range, *Nature*, *418*, 601, doi:10.1038/418601a.

Trigo, R. M., J. M. Vaquero, M.-J. Alcoforado, M. Barriendos, J. Taborda, R. García-Herrera, and J. Luterbacher (2009), Iberia in 1816, the year without a summer, *Int. J. Climatol.*, *29*(1), 99–115, doi:10.1002/joc.1693.

Viechtbauer, W. (2010), Conducting meta-analyses in R with the metafor package, *J. Stat. Software*, *36*(3), 1–48.

Viechtbauer, W. (2012), Meta-analysis package for R, available at: http://www.metafor-project.org (October 2012).

Warnecke, H. (1991), *Meteorologie und Umwelt*, Springer, Berlin.

Wild, M. (2009), Global dimming and brightening: A review, *J. Geophys. Res.*, *114*, D00D16, doi:10.1029/2008JD011470.

Wild, M., A. Ohmura, and K. Makowski (2007), Impact of global dimming and brightening on global warming, *Geophys. Res. Lett.*, *34*, L04702, doi:10.1029/2006GL028031.

Wild, M., B. Trüssel, A. Ohmura, C. N. Long, G. König-Langlo, E. G. Dutton, and A. Tsvetkov (2009), Global dimming and brightening: An update beyond 2000, *J. Geophys. Res.*, *114*, D00D13, doi:10.1029/2008JD011382.

Winkler, P. (2009), Revision and necessary correction of the long-term temperature series of Hohenpeissenberg, 1781–2006, *Theor. Appl. Climatol.*, *98*(3–4), 259–268, doi:10.1007/s00704-009-0108-y.

Yoshimori, M., C. Raible, T. Stocker, and M. Renold (2010), Simulated decadal oscillations of the Atlantic meridional overturning circulation in a cold climate state, *Clim. Dynam.*, *34*(1), 101–121, doi:10.1007/s00382-009-0540-9.